Article ID: 1007-4627(XXXX) 0X-01-010

Comparison of different kernel functions in nuclear charge radius predictions by the kernel ridge regression method

TANG Lu[1], ZHANG Zhenhua[1,2†]

([1]Mathematics and Physics Department, North China Electric Power University, Beijing 102206, China;

[2]Hebei Key Laboratory of Physics and Energy Technology, North China Electric Power University, Baoding 071000, China)

Abstract: Using two nuclear models, i) the relativistic continuum Hartree-Bogoliubov (RCHB) theory and ii) the Weizsäcker-Skyrme (WS) model WS*, the performances of nine kinds of kernel functions in the kernel ridge regression (KRR) method are investigated by comparing the accuracies of describing the experimental nuclear charge radii and the extrapolation abilities. It is found that, except the inverse power kernel, other kernels can reach the same level around 0.015-0.016 fm for these two models with KRR method. The extrapolation ability for the neutron rich region of each kernel depends on the trainning data. Our investigation shows that the performances of the power kernel and Multiquadric kernel are better in the RCHB+KRR calculation, and the Gaussian kernel is better in the WS*+KRR calculation. In addition, the performance of different basis functions in the radial basis function method is also investigated for comparison. The results are similar to the KRR method. The influence of different kernels on the KRR reconstruct function is discussed by investigating the whole nuclear chart. At last, the charge radii of some specific isotopic chains have been investigated by the RCHB+KRR with power kernel and the WS*+KRR with Gaussian kernel. The charge radii and most of the specific features in these isotopic chains can be reproduced after considering the KRR method.

Key words: nuclear charge radius; machine learning; kernel ridge regression method

CLC number: **Document code:** A **DOI:**

1 Introduction

Charge radius is one of the most basic properties of the atomic nucleus. With the improvement of experimental techniques [1, 2], great progress has been achieved in the measurement of the nuclear charge radius, and more than 1000 experimental nuclear charge radii have been obtained [3, 4]. However, this number is still far from enough compared to the possible existing nuclei predicted by various nuclear theories [5, 6]. Charge radius is quite important to understand various nuclear phenomena, such as shell structure [7, 8], shape phase transition [9, 10], the neutron skin and halo [11–13], etc. Therefore, accurate nuclear charge radius predictions are quite important.

Usually, the nuclear charge radius is described by the $A^{1/3}$ law with A the mass number. Thereafter, various phenomenological formulae originated from the $A^{1/3}$ law have been proposed [14–21]. The nuclear charge radius can also be obtained by the nuclear models such as the macroscopic-microscopic models [22–25], and the microscopic models based on the non-relativistic [26–29] and relativistic [6, 30–36] density functionals. Each of these models can give a good description of the nuclear charge radii across the whole nuclear chart. In addition, the local-relation-based models [37–43] are also adopted to predict the charge radius of the unknown nucleus with the information of its existing neighbors.

In recent years, machine learning (ML) has been widely used in nuclear physics [44–46]. Various ML approaches have already been adopted to improve the nuclear charge radius predictions, e.g., the Bayesian neural network [47–51], the artificial neural network [52–54], the radial basis function (RBF) approach [55], the kernel ridge regression (KRR) method [56, 57], etc. By training the ML network with the charge radius residuals, i.e., deviations between the experimental and the calculated nuclear charge radii, the ML methods can reduce the corresponding root-mean-square (rms) deviations to 0.01-0.02 fm.

KRR method is one of the most popular ML methods [58, 59]. It has provided successful descriptions

Received date: XX-XX-XXXX

Foundation item: Natural Science Foundation of China (Grants No. 11875027)

Biography: TANG Lu (1998–), Xuancheng, Anhui province, working on nuclear structure; E-mail: tanglu@ncepu.edu.cn.

[†]**Corresponding author:** ZHANG Zhenhua, E-mail: zhzhang@ncepu.edu.cn.

for various aspects of nuclear physics such as nuclear mass [60–64], nuclear charge radius [56, 57] nuclear energy density functionals [65], neutron-capture reaction cross-sections [66], etc. In these investigations, Gaussian kernel is adopted due to the good extrapolation power, which originates from the decay behavior of the Gaussian kernel with the increasing extrapolation distance. It can automatically identify the limit of the extrapolation distance and avoid the risk of overfitting at large extrapolation distance.

There are a lot of commonly used kernel functions in the KRR method. Recently, Wu has shown that the performances of the KRR approach in nuclear mass predictions can be affected by different kernels [67]. In our previous work, Gaussian kernel is adopted in the KRR or extended KRR method in the nuclear charge radius predictions. So it is necessary to study the performance of the KRR method with different kernels in the nuclear charge radius predictions. In the present work, the performances of the KRR method for nuclear charge radius predictions with nine kinds of kernel functions, including Gaussian, Laplacian, Matern, Cauchy, Multiquadric, inverse Multiquadric, Logarithm, power, and inverse power, are compared by training the radius residuals of relativistic continuum Hartree-Bogoliubov (RCHB) theory [6] and the Weizsäcker-Skyrme (WS) model WS* [4]. For the experimental charge radii of 1014 nuclei with $Z \geq 8$, the rms deviations for RCHB theory and WS* model are about 0.035 fm and 0.021 fm, respectively. The dependence of the kernel functions on the trained data will also be investigated.

This paper is organized as follows. A brief introduction to the KRR method is given in Sec. 2. The results obtained by the KRR method with different kernel functions are given in Sec. 3. With different kernels, the obtained rms deviations by RCHB+KRR and WS*+KRR, and the extrapolation power of the KRR method are compared. In addition, the performance of different basis functions in the RBF method is also investigated for comparison, which is used extensively in nuclear mass predictions with linear basis function [68–72]. Finally, a brief summary is given in Sec. 4.

2 Theoretical framework

The KRR function $S(\boldsymbol{x}_j)$ can be written as

$$S(\boldsymbol{x}_j) = \sum_{i=1}^{m} K(\boldsymbol{x}_j, \boldsymbol{x}_i)\omega_i, \tag{1}$$

where $\boldsymbol{x_i}$ are locations of nuclei in the nuclear chart with $\boldsymbol{x}_i = (Z_i, N_i)$, m is the number of training data, ω_i are weights to be determined, and $K(\boldsymbol{x}_j, \boldsymbol{x}_i)$ is the kernel function, which characterizes the similarity between the data.

By minimizing the following loss function

$$L(\boldsymbol{\omega}) = \sum_{i=1}^{m} [S(\boldsymbol{x}_i) - y(\boldsymbol{x}_i)]^2 + \lambda ||\boldsymbol{\omega}||^2 , \tag{2}$$

the weights ω_i can be determined, where $\boldsymbol{\omega} = (\omega_1, ..., \omega_m)$. The hyperparameter λ ($\lambda \geq 0$) determines the regularization strength and is adopted to reduce the risk of overfitting. Minimizing Eq. (2) leads to

$$\boldsymbol{\omega} = (\boldsymbol{K} + \lambda \boldsymbol{I})^{-1} \boldsymbol{y} , \tag{3}$$

where $\boldsymbol{I}$ is the identity matrix and $\boldsymbol{K}$ is the kernel matrix with elements $K_{ij} = K(\boldsymbol{x}_i, \boldsymbol{x}_j)$.

In the present work, the following nine kinds of kernels are adopted,

$$\text{Gaussian} \quad : \quad K(r) = \exp\left(-r^2/2\sigma^2\right) , \tag{4}$$

$$\text{Laplacian} \quad : \quad K(r) = \exp\left(-r/\sigma\right) , \tag{5}$$

$$\text{Matern} \quad : \quad K(r) = (1 + 3r/5\sigma)\exp\left(-3r/5\sigma\right) , \tag{6}$$

$$\text{Cauchy} \quad : \quad K(r) = 1/(1 + r^2/\sigma) , \tag{7}$$

$$\text{Multiquadric (MQ)} \quad : \quad K(r) = \sqrt{r^2 + \sigma^2} , \tag{8}$$

$$\text{inverse MQ} \quad : \quad K(r) = 1/\sqrt{r^2 + \sigma^2} , \tag{9}$$

$$\text{Logarithm} \quad : \quad K(r) = \ln(1 + r^{\sigma}) , \tag{10}$$

$$\text{power} \quad : \quad K(r) = r^{\sigma} , \tag{11}$$

$$\text{inverse power} \quad : \quad K(r) = 1/r^{\sigma} , \tag{12}$$

where the Euclidean norm

$$r = ||\boldsymbol{x}_i - \boldsymbol{x}_j|| = \sqrt{(Z_i - Z_j)^2 + (N_i - N_j)^2} \tag{13}$$

is defined to be the distance between two nuclei. The σ ($\sigma > 0$) in each kernel is a hyperparameter and its optimal value should be obtained according to the data of the nuclear charge radius.

The KRR function (1) is trained to reconstruct the charge radius residuals $\Delta R(Z,N) = R^{\rm exp}(Z,N) - R^{\rm cal}(Z,N)$. Once the weight parameters w_i are obtained, the KRR function $S(Z,N)$ can be calculated for every nucleus. Therefore, the predicted charge radius for a nucleus (Z,N) is given by $R^{\rm KRR} = R^{\rm cal}(Z,N) + S(Z,N)$.

3 Results and discussion

In the present work, 1014 experimental data with proton number $Z \geq 8$ are considered, which are taken from Refs. [3, 4]. There are 885 data in Ref. [3] and 129 new data in Ref. [4]. In our previous work, the hyperparameters λ had been carefully validated using the leave-one-out cross-validation to be 0.02 for the RCHB+KRR and 0.01 for WS*+KRR [57], and these two values would be adopted in the present work.

The hyperparameter σ in each kernel function is determined by the leave-one-out cross-validation with given λ in the KRR method. The predicted radius for each of the 1014 nuclei can be obtained by the KRR method trained on all other 1013 nuclei with given set of hyperparameters σ and λ. The optimized hyperparameters σ (see Table 1) with given λ can be obtained when the rms deviation between experimental and calculated radii gets its minimum.

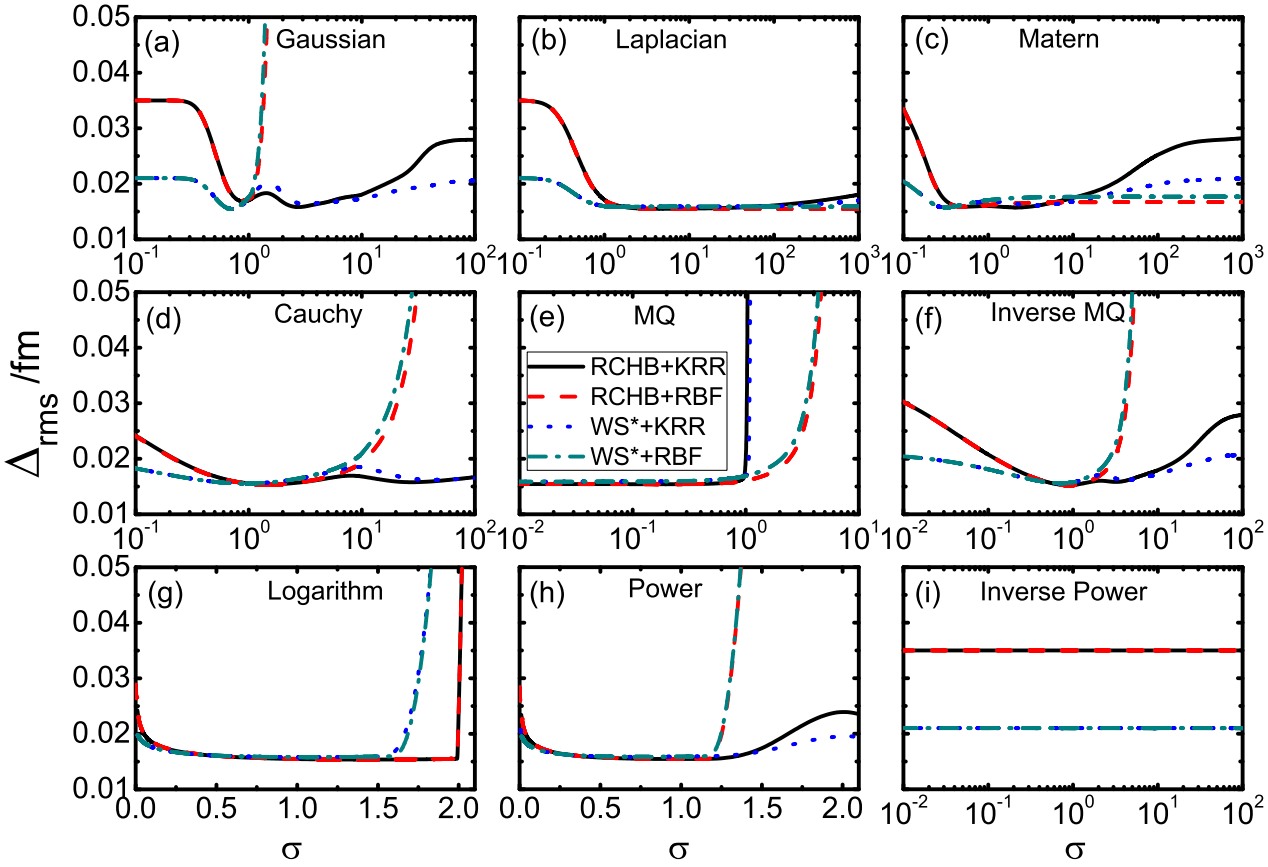

Fig. 1 (color online) The rms-deviations $\Delta_{\rm rms}$ between the KRR/RBF predictions with nine different kinds of kernel functions and the experimental data as functions of the hyperparameter σ. The black solid lines denote the RCHB+KRR results; the red dashed lines denote the RCHB+RBF results; the blue dotted lines denote the WS*+KRR results; the olive dash dotted lines denote the WS*+RBF results.

Figure 1 shows the rms-deviations $\Delta_{\rm rms}$ between the KRR/RBF predictions with nine different kinds of kernel functions and the experimental data as functions of the hyperparameter σ. The black solid lines denote the RCHB+KRR results; the red dashed lines denote the RCHB+RBF results; the blue dotted lines denote the WS*+KRR results; the olive dash dotted lines denote the WS*+RBF results. Table 1 shows the minima of rms deviations $\Delta_{\rm rms}$ and the corresponding optimal hyperparameters σ in the leave-one-out cross-validation for the KRR and RBF approaches with nine different kernel functions as shown in Fig. 1. The notation "all" denotes the total 1014 data; "885" denotes the 885 data in Ref. [3]; "129" denotes the 129 new data in Ref. [4].

It can be seen that, except the inverse power kernel, other kernels can reach the same level around 0.015-0.016 fm for these two models with both KRR and RBF methods. In fact, there is no improvement by the inverse power kernel in all of these calculations. The Gaussian kernel in the RCHB+RBF method is a little larger compared to other calculations. The results indicate that the KRR method with different kernels can reach similar accuracies if proper values of hyperparameters are adopted, and the results are quite similar to the RBF method. Therefore, in the applications of predicting nuclear charge radii for the nuclei that not far away from the experimentally known region, the prediction accuracy may be hardly affected by the choices of the kernel functions. We also can see that the predicted results for the 129 new data are better than the 885 data in Ref. [3]. We also can see that in contrary to the RBF method, the rms deviation obtained by the KRR method does not grow that high for very large σ values except the MQ kernel and the Logarithm kernel. This

demonstrates that the penalty term in the KRR method can prevent overfitting even for very unrealistic kernels.

We can see from Fig. 1 and Table 1 that in these calculations, the parameters σ in MQ kernel $K(r)=\sqrt{r^2+\sigma^2}$ are quite close to zero (especially for the WS* data set), and the σ in power kernel $K(r)=r^\sigma$ are quite close to one (especially for the RCHB data set). Both of these two kernels approach to the linear kernel $K(r)=r$ with the optimized hyperparameter, and their results are quite close to each other. This means that the linear kernel adopted in KRR or RBF method [55] is reasonable in the investigation of the nuclear charge radius.

Tab. 1 The rms deviations $\Delta_{\rm rms}$ (in unit of fm) and the corresponding optimal hyperparameters σ in the leave-one-out cross-validation for the KRR and RBF approaches with nine different kernel functions. The notation "all" denotes the total 1014 data; "885" denotes the 885 data in Ref. [3]; "129" denotes the 129 new data in Ref. [4].

Kernels	Gaussian	Laplacian	Matern	Cauchy	MQ	Inverse MQ	Logarithm	Power	Inverse Power
					RCHB+KRR				
σ	2.68	4.86	2.14	1.52	0.19	0.89	1.43	0.98	-
$\Delta_{\rm rms}$(all)	0.0157	0.0155	0.0157	0.0154	0.0154	0.0152	0.0154	0.0155	0.0350
$\Delta_{\rm rms}$(885)	0.0166	0.0165	0.0167	0.0166	0.0165	0.0163	0.0164	0.0165	0.0361
$\Delta_{\rm rms}$(129)	0.0097	0.0102	0.0100	0.0110	0.0099	0.0105	0.0101	0.0100	0.0260
					RCHB+RBF				
σ	0.86	8.16	0.51	1.48	0.20	0.89	1.45	0.99	-
$\Delta_{\rm rms}$(all)	0.0169	0.0155	0.0159	0.0153	0.0154	0.0152	0.0154	0.0155	0.0350
$\Delta_{\rm rms}$(885)	0.0185	0.0165	0.0171	0.0166	0.0165	0.0163	0.0164	0.0165	0.0361
$\Delta_{\rm rms}$(129)	0.0127	0.0101	0.0106	0.0110	0.0099	0.0105	0.0101	0.0100	0.0260
					WS*+KRR				
σ	0.70	1.66	0.31	0.96	0.01	0.72	1.07	0.76	-
$\Delta_{\rm rms}$(all)	0.0155	0.0158	0.0157	0.0155	0.0159	0.0156	0.0158	0.0158	0.0210
$\Delta_{\rm rms}$(885)	0.0167	0.0169	0.0169	0.0166	0.0169	0.0166	0.0168	0.0168	0.0215
$\Delta_{\rm rms}$(129)	0.0141	0.0121	0.0133	0.0127	0.0114	0.0120	0.0113	0.0113	0.0177
					WS*+RBF				
σ	0.70	1.62	0.31	0.95	0.01	0.72	1.08	0.76	-
$\Delta_{\rm rms}$(all)	0.0154	0.0158	0.0157	0.0155	0.0159	0.0156	0.0158	0.0158	0.0210
$\Delta_{\rm rms}$(885)	0.0167	0.0169	0.0169	0.0166	0.0169	0.0166	0.0168	0.0168	0.0215
$\Delta_{\rm rms}$(129)	0.0141	0.0122	0.0133	0.0127	0.0114	0.0120	0.0113	0.0113	0.0177

To investigate the extrapolation power of the KRR and RBF methods with these nine different kernels, the 1014 nuclei with known charge radii are redivided into one training set and six test sets as follows. For each isotopic chain with more than nine isotopes, the six most neutron-rich nuclei are classified into six test sets according to the distance to the last nucleus. Test set 6 (1) has the longest (shortest) extrapolation distance. The hyperparameters obtained by the leave-one-out cross-validation in Table 1 remain the same in the following calculations.

Figure 2 shows the comparison of the extrapolation ability of the KRR (left panels) and RBF (right panels) methods with eight kinds of kernels and two data sets (RCHB and WS*) for six different extrapolation distances. The results with inverse power kernel are not shown here since there is no improvement by this kernel in all the calculations. It can be seen clearly that with these two different data sets, the extrapolation ability of these kernels are totally different. There is no overfitting in both the KRR and RBF methods when the radius residual in RCHB is adopted, whereas the overfitting appears at extrapolation distance equals to 2 for all the kernels in KRR and RBF methods with WS*. For the RCHB model, the extrapolation ability of KRR method with the power kernel and MQ kernel are better than other kernels. This may be due to the charge radius residual in RCHB model is larger. The predicted KRR function approaches to zero with large extrapolation distance. However, for the WS* model, the charge radius residual is quite smal-

l, overfitting appears when the extrapolation distance gets larger. It can be seen that, among all of these eight kernels, the results with Gaussian kernel are better both in KRR and RBF methods. Therefore, the present results show that the kernel functions or the basis functions in the KRR/RBF method should be checked carefully with given data set. It should be noted that a statistical study of the predictive power of the KRR method is also quite important. However, unlike the Bayesian neural network, it is difficult to introduce the statistical methods in the KRR approach. Previous investigations have shown that if the hyperparameters in the KRR method changed a little, the obtained nuclear mass and charge radii remain nearly unchanged. Therefore, the extrapolation power is not so sensitive to the slight change of hyperparameters.

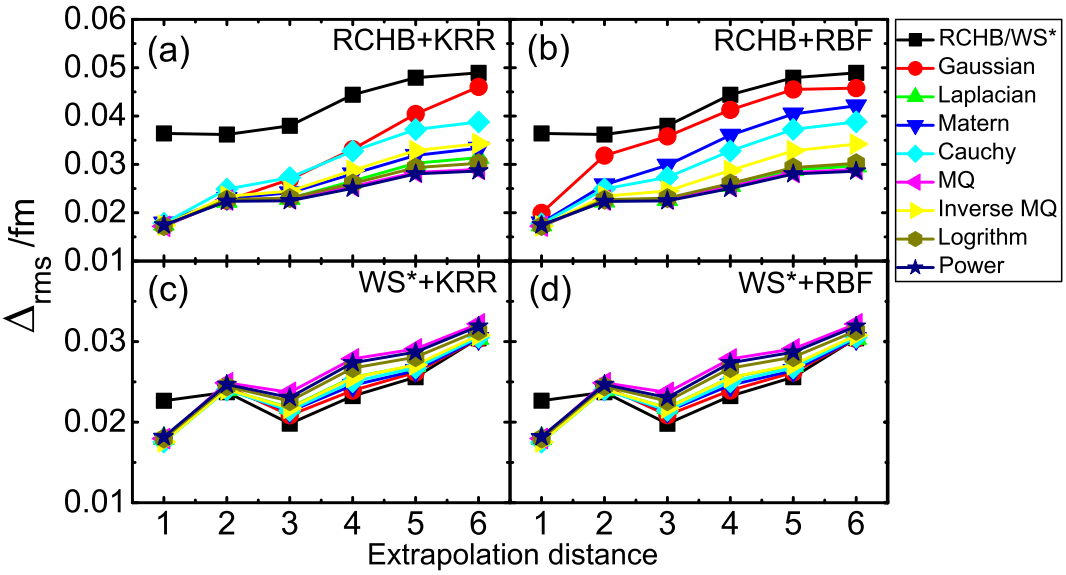

Fig. 2 (color online) Comparison of the extrapolation ability of the KRR (left panels) and RBF (right panels) methods with eight kinds of kernels and two data sets (RCHB and WS*) for six different extrapolation distances.

Since the KRR method with nearly all the kernels can reach the same level for the charge radius prediction, it is quite interesting to study the influence of different kernel functions on the very neutron rich region where no data exists. With the optimized hyperparameters (σ,λ), the reconstructed function $S(N,Z)$ for every nuclei can be calculated by KRR method. Fig. 3 shows the differences $\Delta R = R^{\rm exp} - R^{\rm cal}$ between experimental and the calculated values by RCHB and WS* models (upper panels), the KRR reconstructed function $S(N,Z)$ with power and Gaussian kernels (middle panels), and the differences $\Delta R({\rm KRR}) = {\rm R}^{\rm exp} - ({\rm R}^{\rm cal} + {\rm S}^{\rm KRR})$ between experimental and the predictions of these two models with KRR corrections (lower pannels). It can be seen in Fig. 3(a) and (b) that, the differences between experimental and the calculated values by RCHB model are larger than those for the WS* model. While after considering the KRR corrections, the two patterns of ΔR become quite similar to each other [Fig. 3(e) and (f)]. Fig. 3(c) and (d) show that, the KRR reconstructed function S with the power kernel remains still quite large value even far away from the known region. While for the Gaussian kernel, it become to zero for the very neutron-rich nuclei, which is due to the decay behavior of the Gaussian kernel. It means that for a given nucleus, very little information can be learned from the nuclei far away from it. For comparison, the KRR corrections considered with the Gaussian kernel for RCHB model and power kernel for WS* model are shown in Fig. 4(c) and (d). After considering the different kernels, RCHB+KRR and WS*+KRR still give quite similar ΔR patterns [Fig. 4(e) and (f)], which are also quite close to those in Fig. 3(e) and (f). It can be seen in Figs. 3 and 4 that, if the Gaussian kernel is adopted, the decay behavior of the KRR reconstructed function S is more obvious. The Gaussian kernel can avoid the overfitting to a large extent. However, sometimes the corrections provided by the KRR method with Gaussian kernel maybe not enough compared to other kernels (e.g., the power kernel) if the charge radius residuals are large. Therefore, the adopted kernel is essential to the predicted KRR reconstructed function S in the very neutron-rich region.

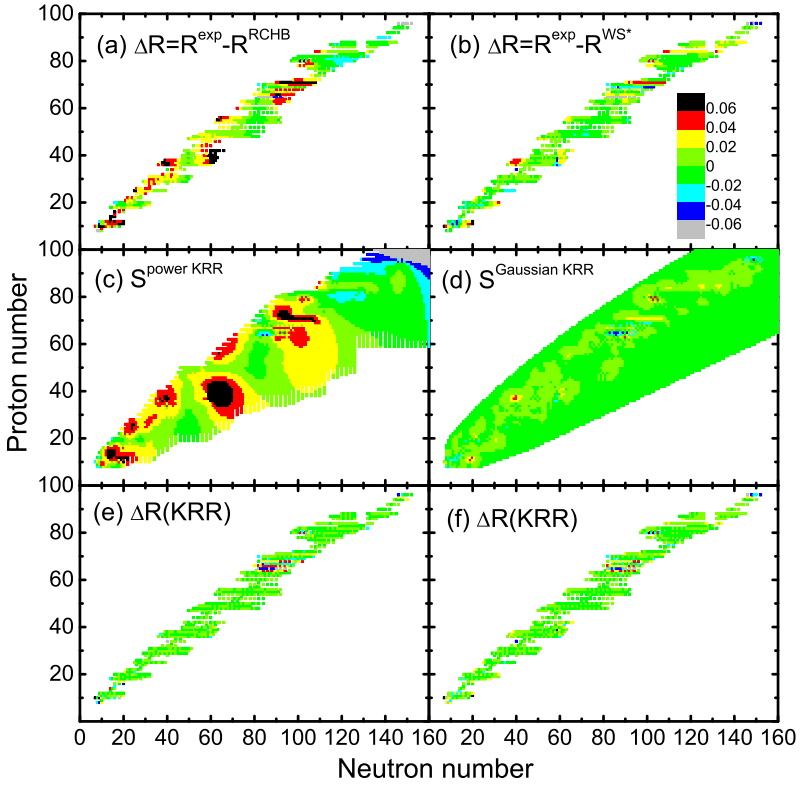

Fig. 3 (color online) The differences $\Delta R = R^{\rm exp} - R^{\rm cal}$ between experimental and the calculated values by RCHB and WS* model (upper panels), the KRR reconstructed function $S(N,Z)$ with power and Gaussian kernels (middle panels), and the differences $\Delta R({\rm KRR}) = {\rm R}^{\rm exp} - ({\rm R}^{\rm cal} + {\rm S}^{\rm KRR})$ between experimental and the predictions of these two models with KRR corrections (lower pannels).

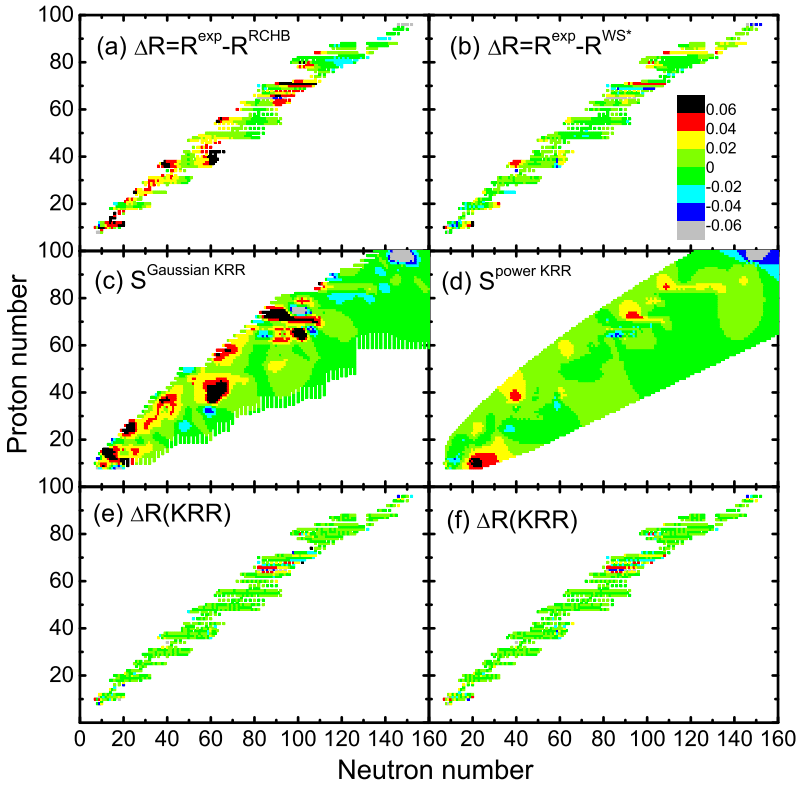

Fig. 4 (color online) The same as Fig. 3, but the KRR corrections are considered with the Gaussian kernel for RCHB model and power kernel for WS* model.

To see the power of the KRR method in describing the nuclear charge radii with the favored kernel functions, Fig. 5 shows the comparison between the experimental and calculated root-mean-square nuclear charge radii for (a) Ne ($Z=10$), (b) Ca ($Z=20$), (c) Zn ($Z=30$), (d) Sn ($Z=50$), (e) Gd ($Z=64$) and (f) Hg ($Z=80$) isotopes. The experimental data are shown by the black solid squares. The calculated results by RCHB (WS*) with and without KRR method using power (Gaussian) kernel are denoted by blue (red) open and solid triangles (circles), respectively. It can be seen in Fig. 5 that in general, the experimental data can be reproduced by RCHB and WS* models. Since only spherical shape is considered in the RCHB model, the deviation between the data and the calculated results is larger than the WS* model for these six isotopes. After considering the KRR method, the results of these two models are both improved and they are quite similar to each other. It can be seen that the odd-even staggering missing in these two models appears with the KRR corrections, especially for the Ca [Fig. 5(b)] and Hg [Fig. 5(f)] isotopes. It should be noted that in most cases, the phases of the calculated odd-even staggerings are opposite to the data and the amplitude is also not quite well reproduced. Our previous investigation shows that after including an odd-even term in the kernel function in the KRR method, the experimental OES could be reproduced quite well [57]. It also can be seen in Fig. 5(d) that in the RCHB model, the calculated charge radii change smoothly when across the neutron $N=82$ shell, and it can not reproduce the abrupt kink at $N=82$. After the KRR method being considered, this kink can be reproduced quite well by the RCHB model. For the proton rich side of Ne isotopes, the charge radii increase drastically with decreasing neutron number, especially for the ^{17}Ne [Fig. 5(a)] . This is due to the existence of the proton halo in this nuclei [73, 74]. It can not be reproduced by the KRR method, which is due to the insufficient of the training data for the halo nuclei.

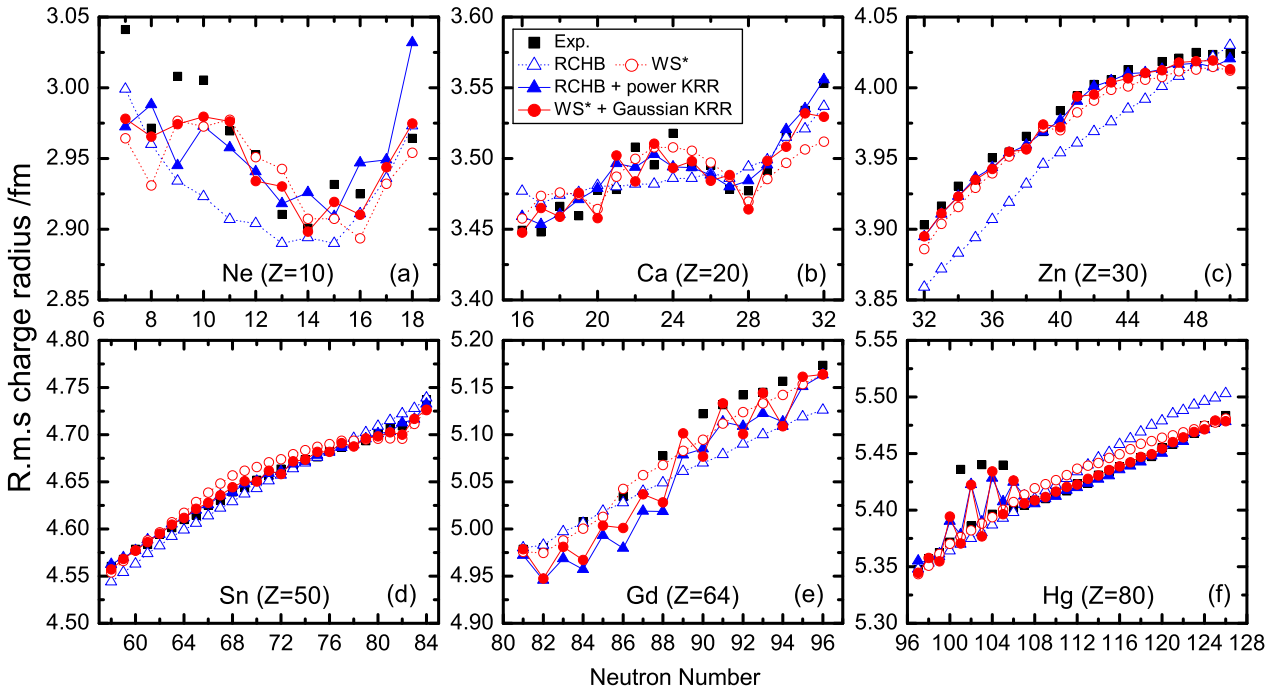

Fig. 5 (color online) Comparison between the experimental and calculated root-mean-square nuclear charge radii for (a) Ne ($Z=10$), (b) Ca ($Z=20$), (c) Zn ($Z=30$), (d) Sn ($Z=50$), (e) Gd ($Z=64$) and (f) Hg ($Z=80$) isotopes. The experimental data are shown by the black solid squares. The calculated results by RCHB (WS*) with and without KRR method with power (Gaussian) kernel are denoted by blue (red) open and solid triangles (circles), respectively.

4 Summary

In this work, the performances of nine kinds of kernel functions in the KRR method are investigated by comparing the accuracies of describing the experimental nuclear charge radii and the extrapolation abilities. Two data sets are adopted, i.e., the RCHB theory and the WS* model. It is found that, except the inverse power kernel, other kernels can reach the same level around 0.015-0.016 fm for these two models with KRR method both with the charge residuals in RCHB theory or WS* model. The results are quite similar to the RBF method. The results indicate that the KRR/RBF method with different kernels can reach similar accuracies if proper values of hyperparameters are adopted. It has been found that the extrapolation ability for the neutron

rich region of each kernel depends on the trained data. Our investigation shows that the performances of the power kernel and Multiquadric kernel are better in the RCHB+KRR and RCHB+RBF calculations. With the optimal hyperparameters, these two kernels are approximate to the linear kernel $K(r) = r$. In the WS*+KRR and WS*+RBF calculations, the Gaussian kernel is better. At last, the charge radii of Ne, Ca, Zn, Sn, Gd and Hg isotopic chains have been investigated by the RCHB+KRR with power kernel and the WS*+KRR with Gaussian kernel. The charge radii and most of the specific features in these isotopic chains can be reproduced after considering the KRR method.

References:

[1] CHEAL B, FLANAGAN K T. J Phys G: Nucl Part Phys, 2010, 37: 113101 http://dx.doi.org/10.1088/0954-3899/37/11/113101

[2] CAMPBELL P, MOORE I D, PEARSON M R. Prog Part Nucl Phys, 2016, 86: 127–180 https://doi.org/10.1016/j.ppnp.2015.09.003

[3] ANGELI I, MARINOVA K. At Data Nucl Data Tables, 2013, 99: 69–95 http://dx.doi.org/10.1016/j.adt.2011.12.006

[4] LI T, LUO Y, WANG N. At Data Nucl Data Tables, 2021, 140: 101440 https://doi.org/10.1016/j.adt.2021.101440

[5] ERLER J, BIRGE N, KORTELAINEN M, et al. Nature, 2012, 486: 509–512 http://dx.doi.org/10.1038/nature11188

[6] XIA X W, LIM Y, ZHAO P W, et al. At Data Nucl Data Tables, 2018, 121-122: 1–215 https://doi.org/10.1016/j.adt.2017.09.001

[7] ANGELI I, MARINOVA K P. J Phys G: Nucl Part Phys, 2015, 42: 055108 https://dx.doi.org/10.1088/0954-3899/42/5/055108

[8] GORGES C, RODRÍGUEZ L V, BALABANSKI D L, et al. Phys Rev Lett, 2019, 122: 192502 https://link.aps.org/doi/10.1103/PhysRevLett.122.192502

[9] WOOD J L, HEYDE K, NAZAREWICZ W, et al. Phys Rep, 1992, 215: 101–201 https://doi.org/10.1016/0370-1573(92)90095-H

[10] CEJNAR P, JOLIE J, CASTEN R F. Rev Mod Phys, 2010, 82: 2155–2212 https://doi.org/10.1103/RevModPhys.82.2155

[11] TANIHATA I, HAMAGAKI H, HASHIMOTO O, et al. Phys Rev Lett, 1985, 55: 2676–2679 http://link.aps.org/doi/10.1103/PhysRevLett.55.2676

[12] TANIHATA I, SAVAJOLS H, KANUNGO R. Prog Part Nucl Phys, 2013, 68: 215–313 https://doi.org/10.1016/j.ppnp.2012.07.001

[13] MENG J, ZHOU S G. J Phys G: Nucl Part Phys, 2015, 42: 093101 https://doi.org/10.1088/0954-3899/42/9/093101

[14] BOHR A, MOTTELSON B R. Nuclear Structure, Vol. I Single-particle Motion. Benjamin, 1969

[15] ZENG J Y. Acta Phys Sin, 1957, 13: 357

[16] NERLO-POMORSKA B, POMORSKI K. Z Phys A, 1993, 344: 359–361 https://doi.org/10.1007/BF01283190

[17] DUFLO J. Nucl Phys A, 1994, 576: 29–64 https://doi.org/10.1016/0375-9474(94)90737-4

[18] ZHANG S, MENG J, ZHOU S G, et al. Eur Phys J A, 2002, 13: 285–289 http://dx.doi.org/10.1007/s10050-002-8757-6

[19] LEI Y A, ZHANG Z H, ZENG J Y. Commun Theor Phys, 2009, 51: 123–125 https://iopscience.iop.org/article/10.1088/0253-6102/51/1/23

[20] WANG N, LI T. Phys Rev C, 2013, 88: 011301(R) https://link.aps.org/doi/10.1103/PhysRevC.88.011301

[21] BAYRAM T, AKKOYUN S, KARA S, et al. Acta Phys Pol B, 2013, 44: 1791–1799 https://www.actaphys.uj.edu.pl/R/44/8/1791/pdf

[22] BUCHINGER F, CRAWFORD J E, DUTTA A K, et al. Phys Rev C, 1994, 49: 1402–1411 https://link.aps.org/doi/10.1103/PhysRevC.49.1402

[23] BUCHINGER F, PEARSON J M, GORIELY S. Phys Rev C, 2001, 64: 067303 https://link.aps.org/doi/10.1103/PhysRevC.64.067303

[24] BUCHINGER F, PEARSON J M. Phys Rev C, 2005, 72: 057305 https://link.aps.org/doi/10.1103/PhysRevC.72.057305

[25] IIMURA H, BUCHINGER F. Phys Rev C, 2008, 78: 067301 https://link.aps.org/doi/10.1103/PhysRevC.78.067301

[26] STOITSOV M V, DOBACZEWSKI J, NAZAREWICZ W, et al. Phys Rev C, 2003, 68: 054312 http://prc.aps.org/abstract/PRC/v68/i5/e054312

[27] GORIELY S, HILAIRE S, GIROD M, et al. Phys Rev Lett, 2009, 102: 242501 http://prl.aps.org/abstract/PRL/v102/i24/e242501

[28] GORIELY S, CHAMEL N, PEARSON J M. Phys Rev C, 2010, 82: 035804 http://prc.aps.org/abstract/PRC/v82/i3/e035804

[29] REINHARD P G, NAZAREWICZ W. Phys Rev C, 2017, 95: 064328 https://link.aps.org/doi/10.1103/PhysRevC.95.064328

[30] LALAZISSIS G A, RAMAN S, RING P. At Data Nucl Data Tables, 1999, 71: 1–40 http://www.sciencedirect.com/science/article/pii/S0092640X98907951

[31] GENG L S, TOKI H, MENG J. Prog Theo Phys, 2005, 113: 785–800 https://doi.org/10.1143/PTP.113.785

[32] ZHAO P W, LI Z P, YAO J M, et al. Phys Rev C, 2010, 82: 054319 http://link.aps.org/doi/10.1103/PhysRevC.82.054319

[33] ZHANG K, CHEOUN M K, CHOI Y B, et al. Phys Rev C, 2020, 102: 024314 https://link.aps.org/doi/10.1103/PhysRevC.102.024314

[34] AN R, GENG L S, ZHANG S S. Phys Rev C, 2020, 102: 024307 https://link.aps.org/doi/10.1103/PhysRevC.102.024307

[35] PERERA U C, AFANASJEV A V, RING P. Phys Rev C, 2021, 104: 064313 https://link.aps.org/doi/10.1103/PhysRevC.104.064313

[36] ZHANG K, CHEOUN M K, CHOI Y B, et al. At Data Nucl Data Tables, 2022, 144: 101488 https://doi.org/10.1016/j.adt.2022.101488
[37] PIEKAREWICZ J, CENTELLES M, ROCA-MAZA X, et al. Eur Phys J A, 2010, 46: 379–386 https://doi.org/10.1140/epja/i2010-11051-8
[38] SUN B H, LU Y, PENG J P, et al. Phys Rev C, 2014, 90: 054318 https://link.aps.org/doi/10.1103/PhysRevC.90.054318
[39] BAO M, LU Y, ZHAO Y M, et al. Phys Rev C, 2016, 94: 064315 https://link.aps.org/doi/10.1103/PhysRevC.94.064315
[40] SUN B H, LIU C Y, WANG H X. Phys Rev C, 2017, 95: 014307 https://link.aps.org/doi/10.1103/PhysRevC.95.014307
[41] BAO M, ZONG Y Y, ZHAO Y M, et al. Phys Rev C, 2020, 102: 014306 https://link.aps.org/doi/10.1103/PhysRevC.102.014306
[42] MA C, ZONG Y Y, ZHAO Y M, et al. Phys Rev C, 2021, 104: 014303 https://link.aps.org/doi/10.1103/PhysRevC.104.014303
[43] LI G S, XU C, BAO M. Chin Phys C, 2023, 47: 084104 https://dx.doi.org/10.1088/1674-1137/acdb54
[44] BEDAQUE P, BOEHNLEIN A, CROMAZ M, et al. Eur Phys J A, 2021, 57: 100 https://doi.org/10.1140/epja/s10050-020-00290-x
[45] BOEHNLEIN A, DIEFENTHALER M, SATO N, et al. Rev Mod Phys, 2022, 94: 031003 https://link.aps.org/doi/10.1103/RevModPhys.94.031003
[46] HE W, LI Q, MA Y, et al. Sci China-Phys Mech Astron, 2023, 66: 282001 https://doi.org/10.1007/s11433-023-2116-0
[47] UTAMA R, CHEN W C, PIEKAREWICZ J. J Phys G: Nucl Part Phys, 2016, 43: 114002 http://dx.doi.org/10.1088/0954-3899/43/11/114002
[48] NEUFCOURT L, CAO Y, NAZAREWICZ W, et al. Phys Rev C, 2018, 98: 034318 https://link.aps.org/doi/10.1103/PhysRevC.98.034318
[49] MA Y, SU C, LIU J, et al. Phys Rev C, 2020, 101: 014304 https://link.aps.org/doi/10.1103/PhysRevC.101.014304
[50] DONG X X, AN R, LU J X, et al. Phys Rev C, 2022, 105: 014308 https://link.aps.org/doi/10.1103/PhysRevC.105.014308
[51] DONG X X, AN R, LU J X, et al. Phys Lett B, 2023, 838: 137726 https://doi.org/10.1016/j.physletb.2023.137726
[52] AKKOYUN S, BAYRAM T, KARA S O, et al. J Phys G: Nucl Part Phys, 2013, 40: 055106 http://dx.doi.org/10.1088/0954-3899/40/5/055106
[53] WU D, BAI C L, SAGAWA H, et al. Phys Rev C, 2020, 102: 054323 https://link.aps.org/doi/10.1103/PhysRevC.102.054323
[54] YANG Z X, FAN X H, NAITO T, et al. Phys. Rev. C, 2023, 108: 034315. https://link.aps.org/doi/10.1103/PhysRevC.108.034315
[55] LI T, YAO H, LIU M, et al. Nucl Phys Rev, 2023, 40: 31. (in Chinese) http://www.npr.ac.cn/cn/article/id/ad4195c3-bd57-49e3-8179-69cde4bb880b
[56] MA J Q, ZHANG Z H. Chin Phys C, 2022, 46: 074105 https://doi.org/10.1088/1674-1137/ac6154
[57] TANG L, ZHANG Z H. Nucl Sci Tech, 2024, 35: 19 https://doi.org/10.1007/s41365-024-01379-4
[58] KIM N, JEONG Y S, JEONG M K, et al. IEEE Trans Syst Man Cybern, 2012, 42: 1011–1020 https://ieeexplore.ieee.org/document/6177683
[59] WU P Y, FANG C C, CHANG J M, et al. IEEE Trans Cybern, 2017, 47: 3916–3927 https://ieeexplore.ieee.org/document/7529146
[60] WU X H, ZHAO P W. Phys Rev C, 2020, 101: 051301(R) https://link.aps.org/doi/10.1103/PhysRevC.101.051301
[61] WU X H, GUO L H, ZHAO P W. Phys Lett B, 2021, 819: 136387 https://www.sciencedirect.com/science/article/pii/S0370269321003270
[62] GUO L, WU X, ZHAO P. Symmetry, 2022, 14: 1078 https://www.mdpi.com/2073-8994/14/6/1078
[63] WU X H, LU Y Y, ZHAO P W. Phys Lett B, 2022, 834: 137394 https://doi.org/10.1016/j.physletb.2022.137394
[64] DU X, GUO P, WU X, et al. Chin Phys C, 2023, 47: 074108 http://iopscience.iop.org/article/10.1088/1674-1137/acc791
[65] WU X H, REN Z X, ZHAO P W. Phys Rev C, 2022, 105: L031303 https://link.aps.org/doi/10.1103/PhysRevC.105.L031303
[66] HUANG T X, WU X H, ZHAO P W. Commun Theor Phys, 2022, 74: 095302 http://dx.doi.org/10.1088/1572-9494/ac763b
[67] WU X H. Front Phys, 2023, 11: 1061042 https://doi.org/10.3389/fphy.2023.1061042
[68] WANG N, LIU M. Phys Rev C, 2011, 84: 051303(R) http://link.aps.org/doi/10.1103/PhysRevC.84.051303
[69] NIU Z M, ZHU Z L, NIU Y F, et al. Phys Rev C, 2013, 88: 024325 http://link.aps.org/doi/10.1103/PhysRevC.88.024325
[70] ZHENG J S, WANG N Y, WANG Z Y, et al. Phys Rev C, 2014, 90: 014303 http://link.aps.org/doi/10.1103/PhysRevC.90.014303
[71] NIU Z M, SUN B H, LIANG H Z, et al. Phys Rev C, 2016, 94: 054315 https://link.aps.org/doi/10.1103/PhysRevC.94.054315
[72] NIU Z M, FANG J Y, NIU Y F. Phys Rev C, 2019, 100: 054311 https://link.aps.org/doi/10.1103/PhysRevC.100.054311
[73] TANAKA K, FUKUDA M, MIHARA M, et al. Phys Rev C, 2010, 82: 044309 https://doi.org/10.1103/PhysRevC.82.044309
[74] ZHANG S S, ZHAO E G, ZHOU S G. Eur Phys J A, 2013, 49: 1–6 http://dx.doi.org/10.1140/epja/i2013-13077-8

核岭回归方法中采用不同核函数对于电荷半径预测的比较

唐璐[1], 张振华[1,2†]

([1]华北电力大学数理学院，北京 102206

[2]河北省物理学与能源技术重点实验室，华北电力大学，保定, 071000)

摘要： 通过采用 i) 相对论连续谱 Hartree-Bogoliubov (RCHB) 理论以及 ii) Weizsäcker-Skyrme (WS) 模型 WS*，本工作比较了在核岭回归 (KRR) 方法中采用 9 个不同核函数对原子核电荷半径描述的精度以及模型的外推能力。本工作发现，在使用 KRR 方法对于电荷半径的描述时，除了逆幂律核，采用其他核函数计算得到的电荷半径的均方根偏差均能达到 0.015-0.016 fm 左右；不同核函数对于丰中子区的外推能力依赖于所采用的数据集。我们的研究表明在 RCHB+KRR 的计算中，幂律核以及多元二次核的外推效果较好；在而 WS*+KRR 的计算中，高斯核的外推效果较好。此外，本文也研究了在径向基函数方法中采用不同类型的基函数对于电荷半径的描述能力，其结果与 KRR 方法类似。随后，通过对整个核素图进行计算，研究了不同核函数对于KRR重构函数的影响。最后，利用考虑幂律核的RCHB+KRR以及高斯核的WS*+KRR方法对一些特定同位素链中原子核的电荷半径进行了研究。考虑KRR方法后，能够很好地再现这些同位素链中原子核的电荷半径以及其中的一些特征。

关键词： 电荷半径；机器学习；核岭回归

收稿日期： XXXX-XX-XX

基金项目： 国家自然科学基金资助项目(11875027)

†**通信作者：** 张振华，E-mail: zhzhang@ncepu.edu.cn